

**AXISYMMETRIC MHD VISCOUS FLOW
ABOUT A SOLID SPHERE TRANSLATING
ALONG THE AXIS OF A SOLID AND MOTIONLESS
CYLINDRICAL TUBE**

A. Sellier^{1*}, *S.H. Aydin*²

¹ *LadHyX. Ecole polytechnique, 91128 Palaiseau Cédex, France*

² *Department of Mathematics. Karadeniz Technical University, 61080, Trabzon, Turkey*
e-Mail: sellier@ladhyx.polytechnique.fr

This work considers the translation of a solid sphere in a conducting Newtonian liquid, bounded by a cylindrical solid and motionless tube with a radius R , subject to a prescribed ambient magnetic field \mathbf{B} . The sphere, with a radius a , has its center located on the tube axis which is parallel to both \mathbf{B} and the sphere velocity. Assuming vanishing Reynolds and magnetic Reynolds numbers, the liquid flow about the sphere, axisymmetric and without swirl, obeys quasi-steady Stokes equations with a Lorentz body force. The stress arising on the sphere surface and the liquid flow are here obtained by truncating the fluid domain, solving coupled boundary-integral equations for the stress axial and radial components and using integral representations for the flow pressure and axial and radial velocity components. A boundary element method is employed to numerically get the drag exerted on the sphere and the flow about it. Both depend on the tube normalized radius R/a and the problem Hartmann number $\text{Ha} = a/d$, where d is the Hartmann layer thickness. The numerical implementation is presented and the computed drag and flow patterns are reported for some settings $(R/a, \text{Ha})$. It is found that, in contrast to the unbounded liquid case, the drag is weakly sensitive to Ha for small Ha and a region of reverse flow takes place near the tube boundary.

Introduction.

Getting the magnetohydrodynamic (MHD) flow about a solid body moving in a conducting, unbounded and quiescent Newtonian liquid subject to a given uniform and steady *ambient* magnetic field $\mathbf{B} = B\mathbf{e}_z$ is a cumbersome task [1, 2]. Actually, this flow and the electric and magnetic fields in the liquid are coupled through the unsteady Navier–Stokes and Maxwell equations by the Lorentz body force. For a liquid with uniform density ρ , conductivity $\sigma > 0$, viscosity μ and magnetic permeability μ_m the problem key numbers are the Reynolds number $\text{Re} = \rho Va/\mu$, the magnetic Reynolds number $\text{Rm} = \frac{\mu_m}{\mu} \sigma Va$ and the Hartmann number $\text{Ha} = a/d$, where a is the body length scale, $d = (\sqrt{\mu/\sigma})/|B|$ is the Hartmann layer thickness [3] and V is the velocity scale. Assuming a body with a magnetic permeability μ_m and $\text{Rm} \ll 1$, the magnetic field in the liquid is then \mathbf{B} (see [4]). Moreover, if the flow is axisymmetric about an axis parallel to \mathbf{B} and *without swirl*, there is no electric field in the liquid [1, 5]. For $\text{Re} \leq O(1)$ one can cite [6], where the steady flow and drag on the sphere are obtained in both Stokes and Oseens limits. Moreover, the MHD flow about the sphere has been numerically investigated (wake, transition) in [7, 8] for Re in the range [10,150]. In this range of Re , the flow is either steady or unsteady, depending on (Re, Ha) . For $\text{Re} \ll 1$, the flow is quasi-steady with a velocity \mathbf{u} and a pressure p subject to the Stokes equations with a Lorentz body force $\mathbf{f}_L = \sigma(\mathbf{u} \wedge \mathbf{B}) \wedge \mathbf{B}$. The resulting MHD flow about a sphere with radius a translating parallel to \mathbf{B} was obtained for small [9], large [10] and arbitrary [11] values of the Hartmann number Ha . This work considers a solid sphere, still translating parallel to \mathbf{B} , immersed in a fluid bounded by a solid and motionless cylindrical tube

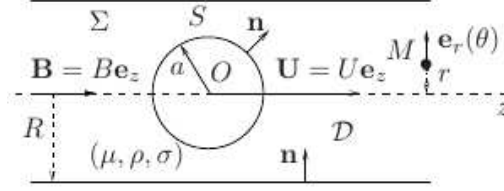


Fig. 1. A solid insulating sphere, with center O , translating in a conducting fluid bounded by a cylindrical solid and motionless tube with the axis $(O, \mathbf{e}_z$. The uniform ambient magnetic field \mathbf{B} and the sphere velocity \mathbf{U} are parallel to the tube axis.

with its axis parallel to \mathbf{B} . This case is solved using the boundary approach introduced and worked out in [11].

1. Addressed axisymmetric problem and asymptotic result.

This section presents the governing problem and derives a useful estimate at small Hartmann number.

1.1. Governing equations and drag coefficient. As shown in Fig. 1, consider a solid sphere with center O , radius a and surface S translating at the velocity $\mathbf{U} = U\mathbf{e}_z$ in a quiescent and conducting Newtonian liquid bounded by a motionless cylindrical tube Σ with radius $R > a$ and axis (O, \mathbf{e}_z) .

The liquid has uniform density ρ , conductivity $\sigma > 0$ and magnetic permeability μ_m . It occupies the domain \mathcal{D} and is subject to the uniform magnetic field $\mathbf{B} = B\mathbf{e}_z$ far from the sphere. Its flow, driven by the sphere motion and the Lorentz body force, has the velocity \mathbf{u} and pressure p . The far-field and no-slip conditions read

$$(\mathbf{u}, p) \rightarrow (\mathbf{0}, 0) \text{ as } |\mathbf{OM}| \rightarrow \infty, \mathbf{u} = U\mathbf{e}_z \text{ on } S \text{ and } \mathbf{u} = \mathbf{0} \text{ on } \Sigma. \quad (1)$$

The flow Reynolds number Re and the magnetic Reynolds number Rm are thus defined as in the Introduction taking $V = |U|$. Henceforth, inertial effects are neglected, i. e. $\text{Re} \ll 1$. This latter condition results for a liquid in $\text{Rm} \ll 1$ so that the magnetic field is \mathbf{B} in the liquid. Since the fluid flow is axisymmetric (about the tube axis) and without swirl, there is no electric field (see the Introduction) and the Lorentz body force is $\sigma(\mathbf{u} \wedge \mathbf{B}) \wedge \mathbf{B}$. Accordingly, (\mathbf{u}, p) satisfies

$$\mu \nabla^2 \mathbf{u} = \nabla p - \sigma B^2 (\mathbf{u} \wedge \mathbf{e}_z) \wedge \mathbf{e}_z \text{ and } \nabla \cdot \mathbf{u} = 0 \text{ in } \mathcal{D}. \quad (2)$$

We shall use cylindrical coordinates (r, z, θ) with the identities $z = \mathbf{x} \cdot \mathbf{e}_z, r = \{|\mathbf{x}|^2 - z^2\}^{1/2} \geq 0$ and $\theta \in [0, 2\pi]$ for any point \mathbf{x} . Thus, $\mathbf{x} = r\mathbf{e}_r + z\mathbf{e}_z$ with a local unit vector $\mathbf{e}_r = \mathbf{e}_r(\theta)$ shown in Fig. 1. Moreover, $\mathbf{u}(\mathbf{x}) = u_r(r, z)\mathbf{e}_r + u_z(r, z)\mathbf{e}_z$ and $p(\mathbf{x}) = p(r, z)$. The flow stress tensor $\boldsymbol{\sigma}$ exerts on the sphere surface, with a unit normal \mathbf{n} pointing into the liquid, the stress $\mathbf{f} = \boldsymbol{\sigma} \cdot \mathbf{n} = f_r(r, z)\mathbf{e}_r + f_z(r, z)\mathbf{e}_z$. Accordingly, the sphere experiences no torque about its center and a force \mathbf{F} parallel to \mathbf{U} and adopting the following form

$$\mathbf{F} = \int_S \boldsymbol{\sigma} \cdot \mathbf{n} dS = [2\pi \int_{\mathcal{C}} f_z(P)r(P)dl(P)]\mathbf{e}_z = -6\pi\mu a C_d \mathbf{U}, \quad (3)$$

with \mathcal{C} being the half-circle trace of S in the $\theta = 0$ half-plane and $C_d > 0$ the drag coefficient. Here, $C_d = C_d(\beta, \text{Ha})$, with $\beta = a/R < 1$ being the tube size parameter and $\text{Ha} = a/d$ the flow Hartmann number (see the Introduction). In addition, the normalized velocity \mathbf{u}/U and the pressure $ap/(\mu U)$ solely depend on $(r/a, z/a)$ and (β, Ha) .

1.2. *Behaviour of the drag coefficient at small Hartmann number.* When the liquid is unbounded ($\beta = 0$), one gets $C_d \sim 1 + 3\text{Ha}/8$ for small Ha [9]. For the present tube case ($\beta > 0$), let $(\mathbf{v}^{(0)}, p^{(0)})$ be the pure Stokes flow obeying Eqs. (1)–(2) for $\sigma B^2 = 0$ (i.e. $\text{Ha} = 0$) and $U = 1$. This flow exerts on the sphere the drag $C_d(\beta, 0)$, which value is given, with a 1×10^{-6} accuracy, in [14]. For small $\epsilon = \text{Ha}^2$, the flow (\mathbf{u}, p) solution to Eqs. (1)–(2) is expanded as $\mathbf{u} \sim U\mathbf{v}^{(0)} + \epsilon\mathbf{u}^{(1)}$ and $p \sim Up^{(0)} + \epsilon p^{(1)}$ with the $(\mathbf{u}^{(1)}, p^{(1)})$ solution to Eqs. (1)–(2) for $U = 0$ and $\mathbf{u}^{(1)}$ replaced with $U\mathbf{v}^{(0)}$ in the right-hand side of the first equation in Eq. (2). This flow $(\mathbf{u}^{(1)}, p^{(1)})$, with a stress tensor $\boldsymbol{\sigma}^{(1)}$, exerts on the sphere the force $F^{(1)}\mathbf{e}_z$. On the tube and sphere surfaces \mathbf{n} is the unit normal pointing into the liquid so that

$$F^{(1)} = \int_S \mathbf{e}_z \cdot \boldsymbol{\sigma}^{(1)} \cdot \mathbf{n} dS = \int_{S \cup \Sigma} \mathbf{v}^{(0)} \cdot \boldsymbol{\sigma}^{(1)} \cdot \mathbf{n} dS = -\frac{\mu U}{a^2} \int_{\mathcal{D}} [\mathbf{v}^{(0)} \cdot \mathbf{e}_r]^2 d\Omega. \quad (4)$$

In Eq. (4) the last equality comes from a reciprocal theorem, with a body force for the flow $(\mathbf{v}^{(1)}, p^{(1)})$, and all integrals exist since from [12] it turns out that $\mathbf{v}^{(0)}$ exponentially decays in magnitude for large $|z|/a$. The force \mathbf{F} exerted on the sphere by the flow (\mathbf{u}, p) reads $\mathbf{F} \sim -6\pi\mu a C_d(\beta, 0)\mathbf{e}_z + \epsilon F^{(1)}\mathbf{e}_z$ so that

$$C_d(\beta, \text{Ha}) \sim C_d(\beta, 0) + \alpha \text{Ha}^2 \text{ for } \text{Ha} \ll 1, \alpha = \frac{1}{6\pi a^3} \int_{\mathcal{D}} [\mathbf{v}^{(0)} \cdot \mathbf{e}_r]^2 d\Omega. \quad (5)$$

For the tube case Eq. (5) shows that the drag increases with small Ha and is also less sensitive to small Ha than for the $\beta = 0$ unbounded liquid case.

2. Advocated boundary method.

The treatment employed in [11] for the unbounded liquid consists in solving coupled boundary-integral equations on the sphere half-circle trace \mathcal{C} . This approach is used for the tube case after truncating the liquid domain. For $L > a$ the truncated liquid domain \mathcal{D}_L has a boundary consisting of the sphere surface S , the $|z| < L$ part Σ_L of the tube Σ and the $z = -L$ and $z = L$ circular cross-sections. The trace of $\partial\mathcal{D}_L \setminus S$ in the $\theta = 0$ half-plane is \mathcal{C}_L and for $\mathbf{x}(r, z)$ in \mathcal{D}_L the associated point in this $\theta = 0$ half-plane is $M(r, z)$. Adopting the tensor summation notation for repeated indices α and β in $\{r, z\}$ and using [11, 13] then yields for (\mathbf{u}, p) satisfying Eq. (1) and the far-field behaviour (2) the following key integral representations

$$u_\alpha(\mathbf{x}) = - \int_{\mathcal{C} \cup \mathcal{C}_L} \left[\frac{G_{\alpha\beta}(M, P) f_\beta(P) r(P)}{8\pi\mu} \right] dl(P) \text{ for } \alpha = r, z \text{ and } \mathbf{x} \text{ in } \mathcal{D}_L \cup \partial\mathcal{D}_L, \quad (6)$$

$$p(\mathbf{x}) = - \int_{\mathcal{C} \cup \mathcal{C}_L} \left[\frac{P_\beta(M, P) f_\beta(P) r(P)}{8\pi} \right] dl(P) \text{ for } \mathbf{x} \text{ in } \mathcal{D}_L \quad (7)$$

with the Green functions $G_{\alpha\beta}(M, P)$ and $P_\beta(M, P)$ given versus $z - z(P), r, r(P)$ and d in [13]. By virtue of Eqs. (6)–(7) the flow is deduced from the knowledge of the stress $\mathbf{f} = f_r\mathbf{e}_r + f_z\mathbf{e}_z$ on $\mathcal{C} \cup \mathcal{C}_L$. The components (f_r, f_z) are obtained by enforcing on $\mathcal{C} \cup \mathcal{C}_L$ the no-slip boundary conditions (2) for u_r and u_z . This yields

$$\int_{\mathcal{C} \cup \mathcal{C}_L} [G_{rr}(M, P) f_r(P) + G_{rz}(M, P) f_z(P)] r(P) dl(P) = 0 \text{ for } M \text{ on } \mathcal{C} \cup \mathcal{C}_L, \quad (8)$$

$$\int_{\mathcal{C} \cup \mathcal{C}_L} [G_{zr}(M, P) f_r(P) + G_{zz}(M, P) f_z(P)] r(P) dl(P) = 0 \text{ for } M \text{ on } \mathcal{C}_L, \quad (9)$$

$$\int_{\mathcal{C} \cup \mathcal{C}_L} [G_{zr}(M, P) f_r(P) + G_{zz}(M, P) f_z(P)] r(P) dl(P) = -8\pi\mu U \text{ for } M \text{ on } \mathcal{C}. \quad (10)$$

Inverting the boundary-integral equations (8)-(10) provides (f_r, f_z) on $\mathcal{C} \cup \mathcal{C}_L$. The flow (\mathbf{u}, p) is subsequently gained in the truncated domain \mathcal{D}_L from Eqs. (6)–(7).

3. Numerical implementation and results.

This section addresses the numerical implementation and presents results for the drag coefficient C_d and the flow.

3.1. Numerical implementation and convergence. Here quadratic curved boundary elements are used on $\mathcal{C} \cup \mathcal{C}_L$ to numerically invert Eqs. (8)–(10). Note that \mathcal{C}_L consists of the trace \mathcal{L}_t of the truncated tube in the $\theta = 0$ half-plane and the end lines \mathcal{L}_- and \mathcal{L}_+ made of points $M(r, z)$ with $0 \leq r \leq R$ and $z = -L$ or $z = L$, respectively. Here we put N_s nodes on \mathcal{C} , N_t nodes on \mathcal{L}_t and N_e nodes on each end line (\mathcal{L}_- or \mathcal{L}_+) so that the typical size of each boundary element is the same on the different curves. One ends up with $N = N_s + N_t + 2N_e$ nodal points on $\mathcal{C} \cup \mathcal{C}_L$ and the discretized counterpart of Eqs. (8)–(9) are enforced at each node, whereas EQ. (10) is only imposed at the $N - 4$ nodes located off the $r = 0$ axis. Indeed, Eq. (10) is trivially satisfied on the axis (because, see [13], $G_{rr}(M, P) = G_{rz}(M, P) = 0$ for $r(M) = 0$). For symmetry reasons, one takes $f_r = 0$ at each node (four nodes actually) on the (O, \mathbf{e}_z) axis. For the given (β, Ha) , the computed drag C_d and flow depend on L/a and the mesh. Some values of C_d for $a/R = 0.4$ are given versus $(L/a, \text{Ha})$ in Table 1.

For this table $N_e = 25, N_t = 101 + 20(L/a - 5)$ and $N_s = 33(65)$ at $\text{Ha} \leq 1 (> 1)$. In agreement with Eq. (5), C_d remains for $\text{Ha} \leq 0.5$ close to the value $C_d = 3.591$ given in [14] for $\text{Ha} = 0$. In addition, the sensitivity to L/a is weak. A few results for $L/a = 7.5$ and some more refined meshes are reported in Table 2.

The values in Table 1 and Table 2 are consistent with a sufficient one percent relative accuracy for the computed drag C_d . Finally, Table 3 summarizes the computed drag at $Ha = 0.01$ for different tubes (with a very fine mesh) and the drag at $Ha = 0$ predicted in [14].

3.2. Numerical results. It is worth considering the drag $C_d(\beta, \text{Ha})$ and the drag normalized by its pure Stokes flow value $\tilde{C}_d(\beta, \text{Ha}) = C_d(\beta, \text{Ha})/C_d(\beta, 0)$. For this work $C_d(\beta, 0)$ is provided in Table 3 from [14]. First, C_d and \tilde{C} are plotted in Fig. 2 versus Ha in $[0, 5]$ for $\beta = 0, 0.4, 0.5$. The drag C_d is seen in Fig. 2a to increase with Ha at the given

Table 1. Computed drag C_d for $\beta = 0.4$ and different values of L/a and Ha .

L/a	$\text{Ha} = 0.01$	$\text{Ha} = 0.1$	$\text{Ha} = 0.5$	$\text{Ha} = 1.0$	$\text{Ha} = 3.0$	$\text{Ha} = 5.0$
5.0	3.593	3.594	3.613	3.672	4.214	5.054
7.5	3.595	3.595	3.615	3.673	4.213	5.027
10.0	3.596	3.597	3.616	3.675	4.215	5.029

Table 2. Computed drag C_d for $\beta = 0.4$ and $L/a = 7.5$ taking $N_s = 64, N_e = 50$ and meshing $[-L/a, L/a]$ with 151 (a) or 301 (b) nodes or meshing each interval $[-L/a, -1], [-1, 1]$ and $[1, L/a]$ with 301 nodes (c).

Mesh	$\text{Ha} = 0.1$	$\text{Ha} = 0.5$	$\text{Ha} = 1.0$	$\text{Ha} = 3.0$	$\text{Ha} = 5.0$
(a)	3.592	3.611	3.670	4.209	5.022
(b)	3.592	3.612	3.670	4.210	5.023
(c)	3.593	3.612	3.671	4.211	5.024

Table 3. Drag C_d for $Ha = 0.01$ (present work) and for $Ha = 0$ [14].

β	0.4	0.5	0.6	0.7	0.8
$Ha = 0.01$	3.592	5.951	11.10	24.73	74.96
$Ha = 0$	3.591	5.947	11.09	24.68	74.67

β and decrease at the given Ha when β increases, i.e. as the tube size decreases. At the given $\beta > 0$, the normalized drag \tilde{C} is shown in Fig. 2b to comply with the theoretical behavior (5). Moreover, \tilde{C} decreases with increasing β at the given Ha .

The trends observed in Fig. 2 survive in Fig. 3 for the narrower tubes $\beta = 0.6, 0.7, 0.8$ except that curves in Fig. 3b now cross.

The flow velocity and pressure have been computed for the previous values of $\beta > 0$ and a few values of Ha . For conciseness, only the results for the axial and radial normalized velocities $\bar{u}_r = u_r/U$ and $\bar{u}_z = u_z/U$ are reported for the $\beta = 0.4$ case ($R/a = 2.5$) and $Ha = 1, 5$. The fluid domain is truncated taking $L/a = 7.5$ although the results are given in the $|z|/a \leq 5$ domain. The computed isovalue curves of the radial normalized velocity \bar{u}_r are first drawn in Fig. 4 using the normalized coordinates $\bar{r} = r/a \geq 0$ and $\bar{z} = z/a$.

Note that, due to symmetries, $\bar{u}_r(\bar{r}, \bar{z}) = -\bar{u}_r(\bar{r}, -\bar{z})$. Moreover, at the given Ha , the quantity $|\bar{u}_r|$ vanishes on both the tube and the sphere contour in virtue of the no-slip boundary condition there. It also quickly decays away from the sphere center and

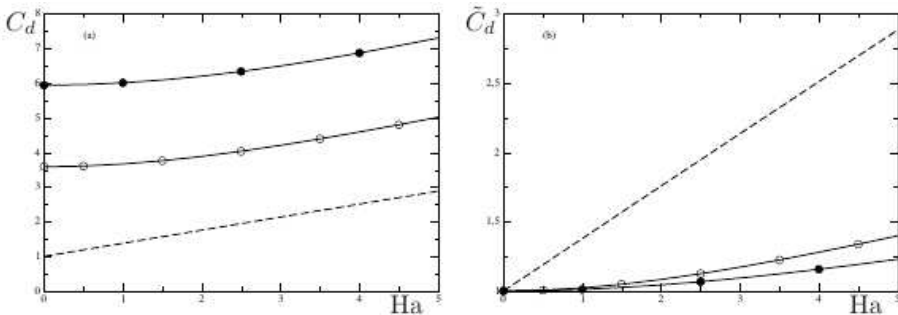


Fig. 2. Drag C_d (a) and normalized drag \tilde{C}_d (b) for $\beta = 0$ (unbounded liquid, dashed line) and $\beta = 0.4$ (○) and $\beta = 0.5$ (●).

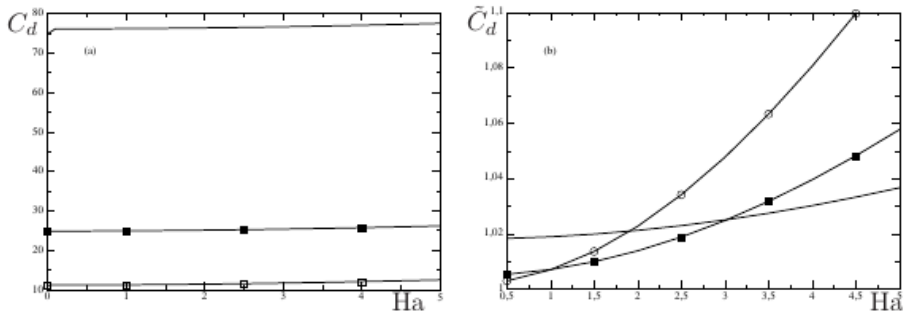


Fig. 3. Drag C_d (a) and normalized drag \tilde{C}_d (b) for $\beta = 0.6$ (open squares), $\beta = 0.7$ (filled squares) and $\beta = 0.8$ (solid line).

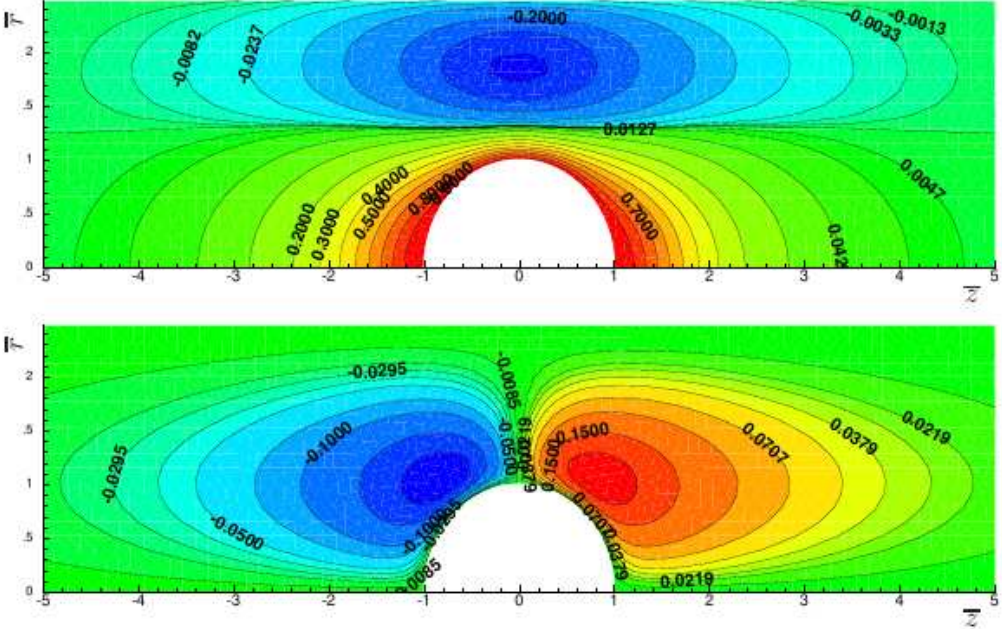


Fig. 4. Isolevel curves of the normalized radial velocity \bar{u}_r for $Ha = 1$ (top) and $Ha = 5$ (bottom) for $R/a = 2.5(\beta = 0.4)$.

remains small in the entire liquid domain. In addition, its largest value is reached in two symmetric pockets located close the sphere. As Ha increases, those pockets extend away from the sphere, i.e. both upstream ($\bar{z} < 0$) and downstream ($\bar{z} > 0$).

The isolevel curves of the axial normalized velocity \bar{u}_z are shown in Fig. 5. For symmetry reasons, this time $\bar{u}_z(\bar{r}, \bar{z}) = \bar{u}_z(\bar{r}, -\bar{z})$. By virtue of the no-slip boundary conditions, \bar{u}_z vanishes on the tube trace and is unity on the sphere half-contour. In contrast to the case of the axial normalized velocity, in the $\bar{z} > 0$ domain the quantity \bar{u}_z changes sign and, therefore, vanishes in the liquid. More precisely, it is negative (region of reverse flow when compared to the sphere translational velocity U) in a pocket located near the tube boundary and the $\bar{z} = 0$ section. As Ha increases, this pockets extends away from the sphere. Note that for the unbounded liquid (case $\beta = 0$ addressed in [11]) one has $\bar{u}_z \geq 0$ in the entire liquid domain. The above-mentioned reverse flow region is due to the no-slip condition on the tube.

Additional flow patterns have been also computed for the more confined cases $\beta = 0.5, 0.6, 0.7, 0.8$. For brevity, the obtained results are not reported. Actually, the normalized velocities \bar{u}_r and \bar{u}_z exhibit the same trend as the ones presented here for $\beta = 0.4$. As β decreases, the thickness of the region of reverse flow close the tube is seen to decrease so that for a small normalised sphere-tube gape $R/a - 1$ one ends up in the flow with a thin layer of negative normalized axial velocity \bar{u}_z . At a given location \bar{z} in the region between the sphere and the close tube \bar{u}_z changes sign when \bar{r} decreases from its value on the sphere contour to zero. There is a high shear $\partial u_z / \partial r = \partial \bar{u}_z / \partial \bar{r}$ there and non-trivial interactions with the Hartmann layer near the sphere contour. This feature makes the flow computation more tricky.

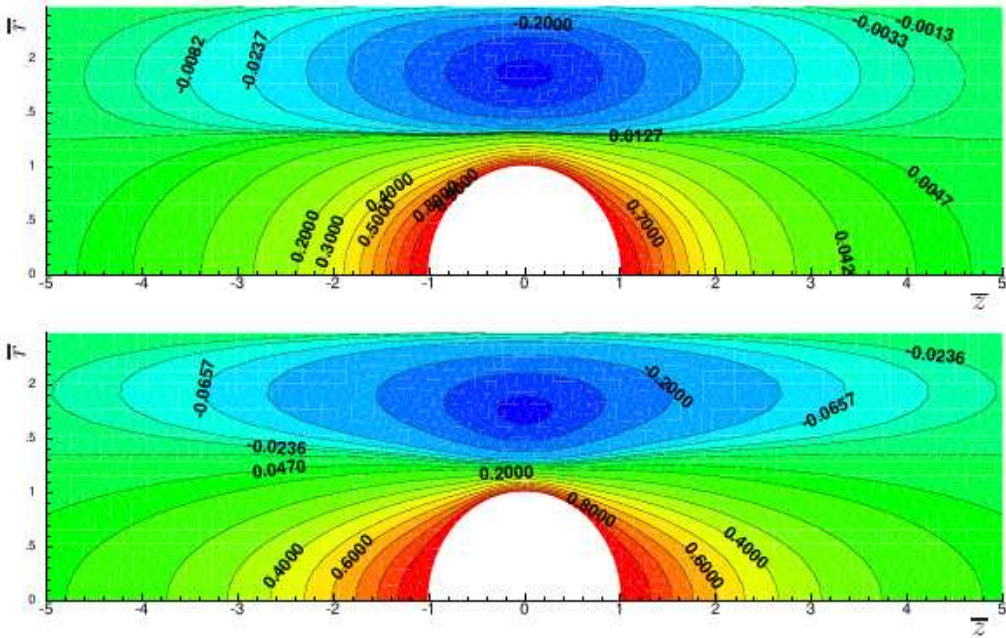


Fig. 5. Isolevel curves of the normalized axial velocity \bar{u}_z for $Ha = 1$ (top) and $Ha = 5$ (bottom) for $R/a = 2.5$ ($\beta = 0.4$).

4. Conclusions.

An efficient and accurate boundary method is presented to calculate the drag exerted on and the MHD axisymmetric flow about a sphere translating in a conducting liquid bounded by a motionless solid cylindrical tube with the axis parallel to both the sphere velocity and the ambient uniform magnetic field applied far from the sphere. The liquid domain is truncated and the procedure reduces to the treatment of coupled boundary-integral equations for the stress radial and axial components on the trace, in a half-plane, of the truncated fluid domain boundary. It is then possible to obtain the fluid velocity and pressure. The numerical implementation uses collocation points and the convergence of the drag coefficient versus the truncation of the fluid domain, and the number of nodes spread on the trace of its boundary is investigated. Moreover, the isolevel curves of the flow normalized radial and axial velocity are reported for two values of the Hartmann number and one tube size. These results (and the calculations for other settings) reveal that, in contrast to the unbounded liquid case, the drag is weakly sensitive to small Hartmann values and there is a reverse flow in the vicinity of the tube.

References

- [1] A.B. TSINOBER. *MHD flow around bodies. Fluid Mechanics and its Applications* (Kluwer Academic Publisher, 1970).
- [2] R. MOREAU. *MagnetoHydrodynamics. Fluid Mechanics and its Applications* (Kluwer Academic Publisher, 1990).
- [3] J. HARTMANN. Theory of the laminar flow of an electrically conductive liquid in a homogeneous magnetic field. *Det Kgl. Danske Videnskabernes Selskab. Matematisk-fysiske Meddelelser*, vol. XV (1937), no. 6, pp. 1–28.

- [4] K. GOTOH. Stokes flow of an electrically conducting fluid in a uniform magnetic field. *Journal of the Physical Society of Japan*, vol. 15 (1960), no. 4, pp. 696–705.
- [5] K. GOTOH. Magnetohydrodynamic flow past a sphere. *Journal of the Physical Society of Japan*, vol. 15 (1960), no. 1, pp. 189–196.
- [6] J.L. BANSAL AND R. KUMARI. MHD slow motion past a sphere. *Proc. Indian Acad. Sci. (Math. Sci.)*, vol. 92 (1978), pp. 157–166.
- [7] J.-H. PAN, N.-M. ZHANG AND M.M.-J. NI. The wake structure and transition process of a flow past a sphere affected by a streamwise magnetic field. *J. Fluid Mech.*, vol. 842 (2018), pp. 248–272.
- [8] J.-H. PAN, N.-M. ZHANG AND M.M.-J. NI. Instability and transition of a vertical ascension or fall of a free sphere affected by a vertical magnetic field. *J. Fluid Mech.*, vol. 859 (2018), pp. 33–48.
- [9] W. CHESTER. The effect of a magnetic field on Stokes flow in a conducting fluid. *J. Fluid Mech.*, vol. 3 (1957), pp. 304–308.
- [10] W. CHESTER. The effect of a magnetic field on the flow of a conducting fluid past a body of revolution. *J. Fluid Mech.*, vol. 10 (1961), pp. 459–465.
- [11] A. SELLIER, S.H. AYDIN. Creeping axisymmetric MHD flow about a sphere translating parallel with an uniform ambient magnetic field. *Magnetohydrodynamics*, vol. 53 (2017), no. 1, pp. 5–13.
- [12] N. LIRON AND R. SHAHAR. Stokes flow due to a Stokeslet in a pipe. *J. Fluid Mech.*, vol. 86 (1978), pp. 727–744.
- [13] A. SELLIER AND S.H. AYDIN. Fundamental free-space solutions of a steady axisymmetric MHD viscous flow. *European Journal of Computational Mechanics*, vol. 25 (2016), issue 1–2, pp. 194–217.
- [14] J.J.L. HIGDON AND G.P. MULDOWNEY. Resistance functions for spherical particles, droplets and bubbles in cylindrical tubes. *J. Fluid Mech.*, vol. 298 (1995), pp. 193–210.

Received 26.11.2024